Minimizing damage during FIB-TEM sample preparation of soft materials

Nabil D. Bassim[1*], Bradley T. De Gregorio[1], A.D.L. Kilcoyne[2], Keana Scott[3], Tsengming Chou[4]†, S. Wirick[5], George Cody[6], and R.M. Stroud[1]

[1]U.S. Naval Research Laboratory, Materials Science and Technology Division, Washington, DC

[2]Advanced Light Source, Lawrence Berkeley National Laboratory, Berkeley, CA

[3]National Institute of Standards and Technology, Gaithersburg, MD

[4]FEI Company, Hillsboro, OR

[5]National Synchrotron Light Source, Brookhaven National Laboratory, NY

[6]Carnegie Institute of Washington, Washington, DC

[*] corresponding author. Code 6366, 4555 Overlook Avenue, SW, Washington, DC, 20375.
Phone: 202-767-2007, nabil.bassim@nrl.navy.mil

[†] current address: Stevens Institute of Technology, Hoboken, NJ

Abstract:

Although focused ion beam (FIB) microscopy has been used successfully for milling patterns and creating ultra-thin transmission electron microscopy (TEM) sections of polymers and other soft materials, little has been documented regarding FIB-induced damage of these materials beyond qualitative evaluations of microstructure. In this study, we sought to identify steps in the FIB preparation process that can cause changes in chemical composition and bonding in soft materials. The impact of various parameters in the FIB-SEM (scanning electron microscopy) sample preparation process, such as final milling voltage, temperature, beam overlap, and mechanical stability of soft samples, was evaluated using two test-case materials systems: polyacrylamide, a low melting-point polymer, and Wyodak lignite coal, a refractory organic material. We evaluated changes in carbon bonding in the samples using X-ray absorption near-edge structure spectroscopy (XANES) at the carbon K edge and compared these samples with samples that had been prepared mechanically using ultramicrotomy. Minor chemical changes were induced in the coal samples during FIB-SEM preparation, and little effect was observed by changing ion-beam parameters. However, polyacrylamide was particularly sensitive to irradiation by the electron beam, which drastically altered the chemistry of the sample, with the primary damage occurring as an increase in the amount of aromatic carbon bonding (C=C).

Changes in temperature, final milling voltage and beam overlap led to small improvements in the quality of the specimens. We outline a series of best practices for preparing TEM samples of soft materials using the FIB with respect to preserving chemical structure and mechanical stability.

Keywords
Focused ion beam, FIB, SEM, TEM, STXM, XANES, damage, soft materials

Introduction:

Focused ion beam microscopy has many advantages over traditional transmission electron microscopy (TEM) sample preparation techniques, primarily the ability to target specific areas for characterization (Giannuzzi & Stevie, 2005). Combination focused ion beam-scanning electron microscopes (FIB-SEMs) can be used for thin section and cross-section preparation of a variety of inorganic, organic, and biological materials. Typically, a 30 keV Ga^+ ion beam is used to sputter materials in such a way as to leave a thin wedge of material at the desired sample site, which must then be detached from the substrate and transferred using a micromanipulator arm to a specialized TEM grid for further thinning. The final thickness is typically less than 100 nm for high resolution imaging. FIB-SEMs offer an additional advantage, related to the geometry of final thinning. Since the pre-thinned, post-transfer, TEM sample is milled to final thickness at a glancing angle, the sample can then be thinned in a manner that allows homogenous thinning of heterogeneous samples (that may have differing sputter yields). This is very useful for TEM characterization, since X-ray yields, electron energy-loss spectroscopy and diffraction contrast images are all easier to interpret for uniformly thin samples.

Some degree of sample surface damage due the irradiation with Ga^+ is inevitable, even for hard materials (Giannuzzi & Stevie, 2005). However, careful attention to the details of the FIB process can minimize artifacts such as redeposition of sputtered material, ion implantation and surface amorphization, and samples of sufficient quality for atomic-resolution high angle annular dark-field studies have been produced. For soft materials (materials that can be deformed thermally at low temperatures), the effects of FIB preparation have even greater potential for physical and chemical alteration of the sample. This beam damage may occur by several mechanisms, including beam-induced heating, knock-on damage and radiolysis.

Beam-induced heating occurs due to the generation of phonons in the sample during cascade collisions. The temperature rise in the sample due to phonons is dependent on the ion beam current, the ion voltage and the thermal conductivity of the sample. Soft materials typically have low thermal conductivities compared to metals or semiconductors (0.5 W/mK - 1 W/mK for polymers and 100 W/mK for Si), and making them more susceptible to beam-induced heating and even melting. Even small temperature increases below the melting point, which result in material softening and a lack of mechanical rigidity during final polishing, can affect the quality of finished TEM sections.

Knock-on damage, in which Ga^+ ions physically displace sample atoms, produces a heavily disordered-to- amorphous surface damage layer (Giannuzzi & Stevie, 2005). The severity of knock-on damage can be directly measured in crystalline samples by determining the width of the amorphous zone at the edge of the sample using high-resolution TEM imaging (HRTEM) (McCaffrey *et al.*, 2001). Soft materials are typically amorphous and also undergo beam damage during evaluation in the TEM, so the surface damage is harder to assess. HRTEM or diffraction contrast would reveal little change, although possible differences in mass-thickness contrast may be visible between the damage layer and the relatively-undamaged sample. Detectable alteration of the surface chemistry could also occur, as knock-on displacements may preferentially remove complete functional groups as a single unit, including entire side groups on long polymer chains.

Radiolysis damage involves irreversible changes in the electronic structure of a material due to incoming ionizing radiation, which can include the destruction of chemical bonds and changes in chemical coordination. Radiolysis in samples can occur from both the electron beam and the charged ion beam. Radiolysis damage in soft materials may result in a change in appearance and the preferential destruction or creation of organic functional groups.

A sample preparation technique that can minimize FIB-induced damage in soft materials has many important applications. Many electrical and optical systems that employ organic materials, such as organic light-emitting diodes (OLEDs), or synthetic hybrid-biological engineered systems, would benefit from reproducible, low-damage, site-specific FIB extraction. Biological studies, such as those of individual cells or bacterial spores are greatly enabled by FIB techniques (Weber *et al., 2010*). Many geological materials containing sub-µm fossil features or other organic matter also require FIB sample preparation (Heaney *et al.*, 2001; Obst *et al.*, 2005;

Schiffbauer & Xiao, 2009). Since these materials are heterogeneous, often with sub-μm ultrastructure, and extremely rare, ensuring minimal damage during FIB preparation is critical.

There are several recent improvements to focused ion-milling technology designed to mitigate damage in FIB-TEM sections (Mayer *et al.*, 2009). These include low-energy (500 V – 2.5 keV) final milling using Ar$^+$ ions (Fischione, 2011) or *in-situ* low-energy (500 V-2 keV) FIB milling using Ga$^+$ ions (Bals *et al.*, 2007). These techniques have been frequently applied to soft materials and their effectiveness has been measured through TEM inspection of the surface amorphous damage layer or implanted defects in the sample. However, applying these damage assessment techniques to beam-sensitive organic and polymeric samples is problematic because TEM observation can itself induce similar damage effects.

Other approaches for reducing FIB-induced damage in soft samples have focused on mitigating the low thermal conductivity of polymeric materials and their inability to dissipate heat during FIB milling. Gianuzzi, Prenitzer and Kempshall (Giannuzzi & Stevie, 2005) suggest that local heating of such samples are confined to interactions that dissipate on the order of picoseconds, and that since the samples are milled with dwell times on microsecond time scales, there ought to be negligible sample heating. However, their study was performed on gold nanoparticles, which has a significantly different thermal conductivity than most polymers. Brostow et al. (Brostow *et al.*, 2007) demonstrated by visual SEM inspection of polymer-matrix composites that reducing the beam overlap as the beam scans from pixel to pixel during FIB milling kept the surrounding polymeric material intact, presumably through the reduction of cascade collisions in the sample and thus reducing beam-induced local heating . Local heating may be further mitigated by preparing block co-polymers with hard/soft interfaces, which have been shown, using TEM, to preserve microstructure of soft material (White *et al.*, 2001). Such hard/soft co-polymers will have more complex, composite heat transfer mechanisms. Kim and Minor (Kim & Minor, 2008) employed a "Shadow FIB" technique for hard/soft interfaces that retain some of the microstructural features of a block co-polymer. Their technique may be useful for preparing samples such as OLEDs, but because it relies on back thinning of the sample, is not as site-specific as a standard lift-out procedure.

Local sample heating may also be reduced by operating the FIB-SEM at cryogenic temperatures. Using cryo-FIB, Marko et al. (Marko *et al.*, 2006) milled into vitreous ice and determined that the milling process itself was not responsible for devitirification. Subsequently,

TEM sections of frozen biological samples were successfully prepared (Marko *et al.*, 2007; Edwards *et al.*, 2009). However, this presents technical challenges not present in a standard TEM lift-out procedure because cryogenic conditions are required at all stages of sample preparation and analysis, including transfer of the sample from the FIB to the TEM.

All of these techniques have demonstrated impressive results in terms of preserving microstructural detail in soft materials. However, there is little assessment of the effectiveness of these techniques for preservation of the original chemistry in the samples. Electron energy loss spectroscopy (EELS) in the TEM may be used to observe FIB-induced changes in sample chemistry, but interactions of high-energy electrons in the TEM beam with beam-sensitive samples may also alter the original chemistry. Synchrotron-based X-ray absorption near-edge structure spectroscopy (XANES), which is analogous to electron energy loss near edge spectroscopy, can also be used to assess subtle changes in carbon functional chemistry. This technique utilizes relatively low energy photons near the electron binding energies of element of interest (~290 eV for C, ~540 eV for O) to probe the inner-shell electron structure of materials and measures characteristic absorption peaks arising from $1s \rightarrow \pi^*$ and $1s \rightarrow \sigma^*$ transitions near these ionization edge energies. This allows fingerprinting of bonding configurations in soft matter samples. Thus, small changes in carbon coordination and functional group chemistry may be observed in FIB samples on a sub-μm scale. Several studies have shown the benefits of XANES over EELS in both conventional TEM and scanning TEM (STEM) with regard to spectral resolution (~0.1 eV) and radiation damage (Hitchcock *et al.*, 2008; Braun *et al.*, 2005a; Braun *et al.*, 2005b). The main disadvantage of this technique as compared to TEM-EELS and STEM-EELS is the relatively low spatial resolution (typically limited to about 25 nm pixel size) and the cost of travel to and maintenance of dedicated STXM synchrotron beamlines. X-ray photons cannot induce atomic displacements in the sample, and the potential for chemical changes due to specimen heating and radiolysis is low (Braun *et al.*, 2005a; Braun *et al.*, 2005b; Wirick *et al.*, 2009; Cody *et al.*, 2009).

Experimental Methods

Two test materials systems, lignite coal and polyacrylamide (PAAm), were studied. These materials are opposite extremes of the range of soft materials that may be selected for FIB

extraction. Coal represents more aromatic and refractory soft materials, and PAAm represents aliphatic O- and N-rich organic matter. In addition, PAAm is very water soluble (and is commonly used as a flocculent), which may mimic unwanted solubility effects observed during typical sample preparation of some type of soft matter (Cody *et al.*, 2008). FIB-based sample preparation may be a more appropriate technique than ultramicrotomy for such water-soluble samples. However, the acrylamide monomer has a low melting point (84 ºC) and the glass transition temperature (T_g) for PAAm is 165 ºC, which may be significantly less than local heating induced by the Ga^+ ion beam. This material then, represents a tough challenge for developing a FIB preparation technique.

We systematically varied parameters of the sample preparation process in order to study the efficacy of recent instrumental advances for reducing beam damage in soft materials, such as the availability of cryogenic FIB, improved optics that allow low-energy final milling, and post-processing using focused Ar^+ ion beams at liquid nitrogen temperatures. The effect of changing sample milling geometry which may encourage electronic and thermal conduction from the sample and increase its mechanical stability was also evaluated.

Changes in chemistry or microstructure due to FIB preparation were evaluated by comparison with 100 nm ultramicrotome sections of both analog materials. Because ultramicrotomy does not involve particle beams or significant sample heating, the microtome sections represent "undamaged" material. However, some structural alteration of the material may be caused by mechanical stresses during microtome sectioning. In addition, we used an ultramicrotomy procedure that relies on lower-temperature embedding of molten sulfur and has been utilized to prepare carbon-containing cosmic dust and cometary particle (originally developed for interplanetary dust particles (Bradley *et al.*, 1993), which involves embedding in molten sulfur droplets rather than traditional epoxy. In this procedure, the sulfur is only heated to slightly above its melting temperature at 115 °C (Meyer, 1976). Since this temperature is below T_g for PAAm and below the observed onset of pyrolysis products in lignite coals, samples should be largely unaffected by the heated droplet. Because PAAm is water-soluble, it was most efficient to create 200 nm - 500 nm sections that are partially dissolved and analyze the thin edges of the sections. Since coal is well known to have μm-scale heterogeneities, the coal section chosen for microtoming was obtained by FIB extraction of a large coupon (10 μm x 10 μm x 10 μm, which was transferred to a microtome stub. A microtome slice from the interior of the

coupon, below the depth of any Ga implantation, was used as the "undamaged" sample. Additional TEM samples were prepared by FIB-milling adjacent to the site of the coupon extraction.

To prepare FIB sections, we used a FEI Nova™ NanoLab 600[1] (Hillsboro, OR) FIB-SEM with the electron beam operated at 5 keV and the ion beam operated at a range of voltages from 30 kV to 5 kV. Particles of coal or PAAm were attached with carbon tape to an aluminum stub and were coated with 200 Å of sputtered gold in order to mitigate sample charging during imaging. A narrow platinum "strap" was first deposited under the electron beam, typically to a thickness of about 500 nm. Then, an additional 1.5 μm of Pt was deposited using the ion beam operated a 0.1 nA, creating a thick protective layer on the top of the sample before further sample imaging and sputtering. Stair-step cross-section mills were then made on either side of the Pt strap, leaving a thick Pt capped section of material in the middle. In typical TEM sample preparation procedures (Overwijk *et al.*, 1993; Giannuzzi *et al.*, 1997), this section is sputtered on both sides until a thickness of ~1 μm is reached, after which the section is detached from the surrounding material and transferred to a special TEM half-grid for further thinning. However, in some special cases our samples were only thinned to 2 μm - 3 μm before this transfer in order to minimize the amount of damage in the center of the section. Total coupon size varied from 5 μm - 20 μm in width to 5 μm – 15 μm in depth.

The samples were Pt welded to a nanomanipulator arm using electron-beam-deposition and transferred to an Omniprobe™ (Dallas, TX) TEM half-grid. The samples were then thinned to electron transparency (~100 nm) using a combination of the following procedures in order to explore the effects of beam energy, beam overlap, sample heating, and sample conductivity: 1) Final beam energy was varied using final thinning mills within the FIB at 30 kV, 5 kV, and 2 kV (coupled with cryo-milling); 2) *Cryo-milling* in a different FEI Nova™ NanoLab 600 FIB SEM equipped with a liquid nitrogen-cooled Quorum Technologies (East Sussex, UK) Polaron-stage operated at 143 K; 3) Focused Ar^+ ion milling with a 5 μm diameter beam at liquid nitrogen temperatures with a final beam voltage of 500 V using a E.A. Fischione (Export, PA) Nanomill™; 4) Rotation of the sample by 360° using an Ascend Instruments (now Omniprobe)

---

[1] Certain commercial equipment, instruments, or materials are identified in this paper to foster understanding. Such identification does not imply recommendation or endorsement by the National Institute of Standards and Technology, nor does it imply that the materials or equipment identified are necessarily the best available for the purpose.

nanomanipulator system, and deposition of a rectangular Pt "frame" around the sample coupon. This experiment was motivated by the potential improvement in charge and thermal conduction away from the sample coupon by a metallic layer to prevent thermal damage and shape change; 5) Differential thinning to leave a thicker frame of native material surrounding a thinner "window" in the sample as a heat sink and source for structural rigidity. Due to its relatively large volume, the thicker bulk material next to the window can absorb the heat generated in the window region, as opposed to a conductive path for the electrons and phonons produced in the thinned sample of the previous case. Again, this experiment is motivated by the desire to suppress thermal damage and structural failure.

The milling rate of the samples significantly increased after transfer to the half-grid because the relatively open geometry of the lift-out coupon reduced the likelihood of redeposition of sputtered material relative to milling into bulk material. As final thinning of the sample progressed, incident ion beam currents were reduced to maintain stable heating rates in the sample and to suppress damage formation.

Sample Characterization

Unwanted mass loss and phase changes (e.g. melting) in soft samples resulting from beam damage during milling are visible as macroscopic physical changes such as warping and bending. Such physical changes in PAAm and coal were characterized using two different SEM instruments, depending on the particular stage of thinning. For samples that were thinned *in-situ* in the FIB, physical changes were observed using FIB-SEM electron beam operated at 5 keV. For samples that were thinned by low-energy Ar^+ milling, characterization of sample thickness, shape, and physical changes was performed in a Hitachi S-4700 SEM operated at 1 keV. Since these soft material analogs may be damaged by electron-beam imaging, measurements of warping or structural failure were often performed from a top-down view using secondary electrons generated by the FIB Ga^+ ion beam to avoid direct electron beam imaging of the broad face of the sample.

Changes in the chemical structure and local bonding of PAAm and coal samples were observed using XANES at several synchrotron facilities. Samples were measured at the 10ID-1 beamline at the Canadian Light Source (CLS), University of Saskatchewan, the X1A1 beamline

at the National Synchrotron Light Source (NSLS), Brookhaven National Laboratory, or the 5.3.2 beamline at Advanced Light Source (ALS), Lawrence Berkeley National Laboratory. Each of these beamlines is equipped with similar STXM instruments, and sample configurations and hardware details are described elsewhere (Kaznatcheev *et al.*, 2007; Warwick *et al.*, 1998; Jacobsen *et al.*, 1991). In short, STXM utilizes Fresnel zone plate optical systems to focus the incident X-ray beam to a ~25 nm probe size (Jacobsen *et al.*, 1992), under which the sample is scanned. By measuring photons transmitted through the sample at each position, X-ray absorption images are generated. All X-ray absorption images in this study were acquired with a 30 nm pixel size, which is large enough to resolve damage layers, if present. A series of STXM images, either two-dimensional images or one-dimensional "line scans", were acquired around the C K-edge (270 eV - 320 eV) with an energy step as small as 0.1 eV (Jacobsen *et al.*, 2000). This energy resolution is nearly an order of magnitude better than typical EELS energy resolution and at least twice as high as that practically achievable in a state-of-the-art TEM (0.3 eV) although with the advent of monochromators in TEM electron sources, that gap is narrowing rapidly. If a given STXM scan includes photoabsorption by the sample, I, and background absorption, I_0, then the XANES optical density, OD, at each photon energy is given by (Stöhr, 1992)

$$OD = -\log\left(\frac{I}{I_0}\right).$$

Photoabsorption peaks in the resulting XANES indicate the presence of unique electronic fine-structure and coordination due to the local bonding environment of carbon atoms, and XANES spectra may be interpreted similarly to EELS spectra. For example, aromatic carbon-carbon double bonds (C=C) generate a photoabsorption peak around 285.2 eV, while nitrile functional groups (C≡N) generate a distinct peak at 286.6 eV. Other XANES photoabsorption peaks are tabulated in Cody et al. (2008). All XANES calculations and background subtraction was performed using the aXis2000 software package (aXis2000, 2011).

Results and Discussion:

Undamaged Material

Ultramicrotome sections of PAAm and lignite coal serve as the "undamaged" control material to which all FIB-prepared samples will be compared. XANES spectra of these undamaged samples are presented in Figure 1. Both PAAm and coal contain distinct populations

of π-bonded carbon atoms, which are visible as characteristic 1s $\rightarrow$ π^* transitions in their XANES spectra. The spectrum of PAAm (Figure 1b) shows the presence of amide side groups (NH_2-C=O) by a singular photoabsorption at 288.0 eV. As expected for a saturated polymer backbone, there is no significant peak around 285 eV, which would correspond to the presence of aromatic or olefinic (C=C) bonding. Minor intensity is present at 284.9 eV, which may be due to a small amount of polymer cross-linking, carbon deposition during STXM analysis, or perhaps damage from the incident X-rays. In contrast, three different primary peaks are identifiable in the XANES spectrum of coal, which correspond to a high proportion of aromatic bonds (285.2 eV), aromatic ketones (286.6 eV) and carboxyl functional groups (288.5 eV). These three peaks are typically observed in coals and related kerogens (Cody *et al.*, 1998; Bernard *et al.*, 2009).

Effect of Electron Beam Irradiation

.   In order to study the effect of the radiation damage due to the electron beam, we imaged samples at extraction voltages of 5 keV or 1 keV during standard FIB preparation. In addition, some samples were also milled without electron beam imaging during final thinning after the sample had been transferred to the TEM half-grid.

The effect of electron imaging on lignite coal chemistry and carbon bonding is shown in Figure 2. These samples were milled with a 30 kV Ga+ ion beam down to a final section thickness of ~100 nm. Qualitatively, all of the XANES photoabsorption peaks that are present in the undamaged ultramicrotomed section are also present in FIB-prepared sections with and without electron beam imaging. However, the relative peak heights change slightly, which may be used to estimate the degree of chemical change between samples. Semi-quantitative comparison was made by fitting three fixed-width Gaussian distributions to each of the three photoabsorption peaks, and a Gaussian error function to model the K-edge "step" above 290 eV. Then the normalized peak intensity of each Gaussian should be proportional to the abundance of each organic functional group or local bonding environment. Although exact quantification of functional group abundance is not trivial due to uncertainties in sample thickness, differences in photon absorption coefficients and the presence of thin amorphous damage layers on FIB-prepared sections, peak ratios may be reasonably compared between samples. Intensity ratios of aromatic carbon, aromatic ketone, and carboxyl group photoabsorptions (Table 2) indicate that aromatic ketones are more abundant, relative to aromatic carbon and carboxyl groups, in FIB-

prepared samples. In addition, aromatic ketones are more abundant in samples which were imaged with the SEM beam during final thinning.

An additional peak at 290.7 eV is present in the XANES spectrum of ultramicrotomed coal, which may correspond to absorption due to carbonate (CO_3) functional groups. This additional peak may indicate the presence of either organic carbonate esters or discrete carbonate minerals within the lignite. Lignite coal is the least mature, most highly oxygenated class of coal and the presence of carbonate esters should not be unexpected. SEM imaging during FIB preparation revealed a heterogeneous microstructure with small secondary phase particulates present within the coal. STXM imaging of the microtomed coal samples did not show the presence of distinct carbonate minerals, which would generate a distinct XANES spectrum, suggesting that either the carbonate grains are smaller than about twice the resolution of the STXM instrument (~50 nm) or carbonate grains are not responsible for the additional peak at 290.7 eV. Other coal samples also contain this carbonate peak, but there is no systematic correlation with the presence or absence of that functionality based on the experimental parameters. Rather, we believe this peak arises from oxygen-rich areas within the heterogeneous microstructure of our coal sample.

Sample	$I_{ketone}/I_{aromatic}$	$I_{carboxyl} / I_{aromatic}$	$I_{ketone}/I_{carboxyl}$
Microtome	1.017	1.379	0.737
No electronbeam	1.032	1.171	0.881
5 keV electron beam	1.067	1.146	0.931

Table 1: XANES peak intensity ratios.

We used the CASINO Monte Carlo simulation package (Drouin *et al.*, 2007) (using Bakelite as the standard reference material) to determine that 5 keV electrons should penetrate about 400 nm deep into the sample. This indicates that a FIB-extracted coal sample should be at least 1 μm thick in order to avoid any potential electron-related damage to a 200 nm thick "core" in the center of the section. Sample manipulation or ion-beam thinning performed on samples thinner than 1 μm should be performed without electron imaging. Alternatively, electron imaging with a 1 keV beam (in a well-aligned electron microscope) opens the possibility of the

extraction of a thinner sample, since the electron penetration depth reduces to 30 nm. This may be useful for the small samples, < 300 nm, including thin films or nanoparticles.

The effect of electron beam irradiation on polyacrylamide (Figure 3) is much more dramatic than on lignite. The XANES spectrum of microtomed PAAm, representing "undamaged" baseline specimen, is dominated by a very intense peak at 288.0 eV corresponding to the presence of abundant amide functional groups ($O=C-NH_x$), with a very slight peak at 285 eV corresponding to aromatic C=C (Figure 3a). In each of the FIB-prepared samples (Figure 3 b-e), two additional peaks are visible at 286.6 eV and 289.2 eV, corresponding to the nitrile ($-C\equiv N$) and the imine (C=N-C) functional groups, respectively. The aromatic, nitrile, and imine peaks grow in intensity at the expense of the amidyl moiety as a function of increasing electron beam voltage. Amide functionality may be transformed into these other moieties by the sequential loss of hydrogen and the occasional removal of hydroxyl (OH). Studies of TEM beam damage of epoxy and cyanoacrylate have also shown that hydrogen removal can cause significant chemical changes, including a relative enrichment of deuterium in the sample (De Gregorio *et al.,* 2009)

For one of the FIB-prepared PAAm samples, SEM was only used to navigate the sample to locate an appropriate position for protective Pt deposition. After the first Pt "strap" was deposited using the electron beam (5 kV, 1.6 nA) there was no further exposure of the sample to the electron beam. All the remaining steps of the FIB-preparation process, including transfer to an Omniprobe TEM half-grid at a thickness of 2.5 μm and final milling down to electron transparency (~100 nm), were performed using only the ion beam. However, the use of the electron beam for the Pt deposition created a layer of damaged PAAm at the top of the resulting FIB section, directly under the Pt strap (Figure 3f). Because of the distinct X-ray absorption properties between this damaged layer and the underlying "pristine" PAAm, the damage layer is visible in STXM images of the section, extending 420 nm below the Pt strap.

Monte Carlo simulations of 5 keV electrons indicate that the penetration depth into PAAm should be about 850 nm (Drouin *et al.,* 2007), roughly twice the depth of the measured damaged layer. One possible explanation for this discrepancy is that the electron beam induced alteration may itself increase the density of the sample, limiting the range of the incident electrons. It should be noted, that at least at 5 keV in these soft materials, electron deposition of the protective strap is more damaging that ion beam deposition. For 1 keV electrons, we

calculate a penetration depth of about 58 nm, which suggests that electron beam deposition of the Pt mask at 1 kV may be more comparable to the surface damage from ion beam deposition.

For both the coal and the PAAm, hydrogen loss appears to be the main mechanism for chemical change, increasing as a function of electron irradiation. Taking potential sample damage due to electron irradiation into consideration, in order to prepare high-quality TEM specimens which preserve original chemistry, extreme care should be taken to use electron imaging sparingly when performing a FIB lift-out. In addition, the minimum section thickness which may be exposed to the electron beam may be estimated by simulating the penetration depth of electrons into the sample material.

Effect of final ion milling voltage on functionality

A series of experiments was done to observe the potential alteration of chemistry in soft samples due to ion beam energy during final milling. Since electron irradiation had such a significant effect on the functional chemistry of the final samples, this series of lift-outs was performed without SEM imaging after the section had been thinned to 1 μm - 2 μm. Various final polishing ion voltages were used, and some samples were thinned using 500 V Ga+ ions in a Fischione Nanomill at liquid nitrogen temperatures.

The chemical functionality of coal samples that were prepared by cryo-FIB are shown in Figure 4. These samples display all of the photoabsorption peaks that were present in the samples that had been prepared using SEM imaging. The relative intensity of the aromatic carbon, ketone, and carboxyl peaks is not significantly different between the FIB-prepared samples as a function of final ion beam voltage. All of the samples display an increase in ketone photoabsorption compared to the pristine microtomed control sample. Some of the FIB-prepared samples also show additional photoabsorption at 290.7 eV, which is likely due to the presence of either carbonate esters or sub-μm carbonate grains. Qualitatively, the XANES spectra indicate that some hydrogen loss may still occur during the FIB-preparation process, even in the absence of electron beam imaging. However, since there is little spectral difference between pristine coal and FIB-prepared coal samples (without SEM imaging), it is likely that lignite coal and other refractory carbonaceous matter are relatively robust under the ion beam.

The effect of final polishing ion voltage on PAAm in the absence of SEM imaging is shown in Figure 5. Compared to the effects associated with the electron radiolysis of carbon-hydrogen bonds in PAAm, the effect of varying incident ion voltage is quite modest. There is a small increase in the abundance of aromatic carbon as a function of increasing final milling voltage. In addition, X-ray absorption due to nitrile and imine moieties also increases slightly when final milling voltage is increased. These observations suggest that knock-on damage due to Ga+ ions during FIB-preparation also contributes to hydrogen loss in the sample, leading to the formation of aromatic, nitrile, and imine bonding. However, these chemical changes are minor compared to the effect induced by electron irradiation.

Since final milling is performed at glancing incidence, the penetration depth of 30 kV Ga+ ions is much less than the final thickness of the section. Therefore, the chemical alteration caused by knock-on damage is likely constrained to thin surface damage layers on both surfaces of the section, with a relatively undamaged "core" of material in the center of the section. Since lowering the voltage of the Ga^+ beam lowers the penetration depth of the ions, it is likely that the observed correlated chemical changes indicate the presence of thinner damage layers relative to undamaged bulk PAAm. A similar reduction of amorphous damage layers have been observed in FIB-prepared sections of crystalline materials by using low-energy final polishing(Giannuzzi *et al.*, 2005). Because XANES analyses are performed by transmission of X-rays through the sample, these damage layers cannot be directly measured but can only be inferred by deviations from pristine chemical functionality in the sample. Polymer damage layers may be observable by TEM, but PAAm and many other polymers will quickly succumb to radiolysis damage from the electron beam before the measurement can be accomplished. However, it may be possible to measure the depth of Ga implantation at the sample edge using HAADF imaging in order to infer the relative penetration of the sample.

Effect of beam heating on the PAAm

Aside from direct damage effects from the electron and ion beams, sample interaction with particle beams can generate localized heating, which may also have a significant effect on organic materials with low melting temperatures. We compared a PAAm, our low T_g analog, FIB lift-out that was not imaged by SEM below 1.5 μm thickness and was final-polished with 30 kV Ga^+ ions to a series of control sections that had been microtomed following vacuum annealing

above the glass transition temperature of the polymer in order to examine various methods of mitigating local sample heating. No significant changes in chemical functionality of the annealed PAAm were observed with XANES, up to an annealing temperature of 231 °C (Figure 6). All of the annealed PAAm are spectrally distinct from FIB-prepared material, which show modest photoabsorption due to increasing amounts of aromatic, nitrile, and imine carbon bonding. This indicates that bulk sample heating and softening does not necessarily lead to significant changes in functional chemistry in low melting point materials.

During FIB-preparation, PAAm sections clearly manifested several effects of sample softening (Figure 7). Typically, sections started to warp and curl into the Ga+ beam (Figure 7b). This warping usually begins from the lower outside corner of the section, furthest away from the TEM grid post and the Pt strap at the top of the section (Figure 7a).

Sample rigidity can be maintained by the presence of a "frame" of thicker material surrounding the thinned region of interest. This can be accomplished by either depositing Pt on the remaining three sides of the section prior to attachment to the TEM grid post (Figure 7c, e) or leaving a thick boundary of sample material as a "natural frame" (Figure 7d, f). Both types of framing methods provide a local heat sink for ion- and electron-generated phonons in the sample to minimize the amount of sample heating in the thinned "window". In addition, the Pt frame may act as a conduction path for electrons to escape from the samples through the TEM grid, thus reducing the amount of radiolysis damage. Lift-out sections of PAAm prepared with either a Pt frame or natural frame were equally effective in maintaining the rigidity and mechanical integrity of the sections (Figure 7e, f).

Adding Pt frames does have several significant drawbacks: an increased damage to the section with an increased use of the electron beam to rotate the sample and additional electron beam imaging. In addition, this is an extremely time-consuming operation and depends heavily on operator skill. Natural framing is certainly much faster but requires a keen understanding of milling rates in the sample at glancing angle geometry.

The amount of local heating generated by an incident ion beam during milling (Orloff, 2009) is equal to

$$\Delta T \ = \ \frac{JV}{2k} r_0$$

where V is the accelerating voltage of the incoming Ga^+ beam of radius r_0 at the sample, k is the thermal conductivity of the sample, and the current density J is given by

$$J = \frac{I}{\pi r_0^2}$$

where I is the incident beam current. Calculated specimen heating for several cases are given in Table 2, assuming values of k_{coal} = 0.41 W/m°K (Herrin & Deming, 1996) and k_{PAAm}=0.56 W/m°K (Davidson & Sherar, 2003).

Material	Voltage (kV)	Current (pA)	Beam Diameter (nm)	ΔT (K)
Coal	30	1000	99	234
Coal	30	300	66	106
Coal	30	30	32	22
Coal [a]	5	150	96	6
Coal [b]	0.9	231	6000	0.1
PAAM	30	1000	99	171
PAAM	30	300	66	77
PAAM	30	30	32	16
PAAM [a]	5	150	96	4
PAAM [b]	0.9	231	6000	0.1

Table 2: Calculated maximum local heating for various ion beam parameters in the FIB.

[a]Values calculated using the FEI Sidewinder ion column operated at 5 kV

[b]Values calculated using the Fischione Nanomill

These estimated temperature increases can be much greater at higher beam currents, and can elevate the temperature of the sample past T_g for soft polymer materials such as PAAm. As a result of the incident ion beam, much of the material that is exposed to these temperatures is sputtered away, removing most of the observable thermal degradation. Nevertheless, some heat diffuses to the adjacent material towards the interior of the section and this can cause sample softening. During the early stages of FIB milling (i.e. coarse cutting), the temperature rises about 171 °C. This temperature rise decreases as a function of distance and falls below 100 K within 40 nm (Orloff, 2009). The final polishing steps, when the section is thinnest, are the most critical in terms of beam induced heating in soft samples, and beam currents as low as reasonably

possible should be used. Fortunately, reasonable final polishing voltages and currents should not generate enough heat to cause a phase transition in PAAm or coal.

Modifying the "overlap" of the Ga+ beam during FIB milling has also been suggested as another method of mitigating sample heating (Brostow *et al.*, 2007). Beam overlap is a parameter that may be changed in most FIB control software and specifies how closely-spaced adjacent beam positions are as the beam is rastered across the sample. This has the effect of separating successive ion cascade collisions and, in the beam heating model described above, would correspond to a *de facto* decrease in beam current. A sample that was prepared by reducing the ion beam overlap parameter (from 50% to 0%) shows a modest decrease in the abundance of aromatic C=C bonding (Figure 8). This implies that some of the observed damage may be thermally generated, perhaps through the local volatilization of hydrogen or amide side-chains from the polymer. Although this effect is negligible for PAAm, In general, it is advisable to reduce the ion beam overlap when milling of soft samples and polymers as a straightforward way to lower the incident beam current on the sample.

Conclusion

We used FIB to prepare electron- and X-ray-transparent cross-sections of "soft" carbonaceous materials. Synchrotron-based XANES spectroscopy allowed the evaluation of FIB-induced changes in functional chemistry of amorphous and beam-sensitive analog samples without relying on TEM or other high-energy techniques that can potentially damage soft samples during analysis. Observed changes in functional chemistry of PAAm and coal are related to fundamental FIB parameters such as final ion voltage, ion beam overlap, and the use of electron-beam irradiation for viewing the sample during thinning. The two materials systems in this study behaved quite differently, with the variation of most FIB parameters having little effect on the functional chemistry of the more refractory coal samples. Of these parameters, the use of SEM imaging while preparing cross-sections induced a considerable amount of chemical damage in PAAm, likely mostly due to hydrogen loss during electron irradiation. This does not preclude the preparation of FIB lift-out sections, though, since most electron-induced damage can be avoided by using low electron beam voltages, transferring a much thicker lift-out section (1 μm - 2 μm) to the TEM half-grid, and refraining from using the electron beam to visualize the sample during

the final polishing steps. While beam-induced heating was not observed to play a critical role in the potential alteration of functional chemistry, it has a profound effect on mechanical stability in the lift-out sections. We have demonstrated several practical approaches for minimizing local specimen heating and mechanical failure, including to the use oflower ion beam currents during final milling, lower the ion beam overlap parameter and a rigid Pt or natural frame around the thinned region of interest. A small reduction in the amount of aromatic C=C bonding of PAAm sections from changing final ion voltages indicates that there is a thin layer of damaged material on the surface of the lift-out sections that may be polished away.

References:

aXis 2000 (2011) http://univorn.mcmaster.ca/aXis2000.html. Last accessed 1/4/2011.

Bals, S., Tirry, W., Geurts, R., Yang, Z. Q. & Schryvers, D. (2007) High-quality sample preparation by low kV FIB thinning for analytical TEM measurements. *Micros. Microanal.,* **13,** 80-86.

Bernard, S., Benzerara, K., Beyssac, O., Brown Jr, G. E., Stamm, L. G. & Duringer, P. (2009) Ultrastructural and chemical study of modern and fossil sporoderms by Scanning Transmission X-ray Microscopy (STXM). *Review of Palaeobotany and Palynology,* **156,** 248-261.

Bradley, J. P., Keller, L. P., Thomas, K. L., Vander Wood, T. B. & Brownlee, D. E. (1993) Carbon analyses of IDPs sectioned in sulfur and supported on beryllium films. Abstracts of the 24th Lunar and Planetary Science Conference, Houston, TX. p. 173.

Braun, A., Huggins, F. E., Shah, N., Chen, Y., Wirick, S., Mun, S. B., Jacobsen, C. & Huffman, G. P. (2005a) Advantages of soft X-ray absorption over TEM-EELS for solid carbon studies - a comparative study on diesel soot with EELS and NEXAFS. *Carbon,* **43,** 117-124.

Braun, A., Shah, N., Huggins, F. E., Kelly, K. E., Sarofim, A., Jacobsen, C., Wirick, S., Francis, H., Ilavsky, J., Thomas, G. E. & Huffman, G. P. (2005b) X-ray scattering and spectroscopy studies on diesel soot from oxygenated fuel under various engine load conditions. *Carbon,* **43,** 2588-2599.

Brostow, W., Gorman, B. P. & Olea-Mejia, O. (2007) Focused ion beam milling and scanning electron microscopy characterization of polymer plus metal hybrids. *Materials Letters,* **61,** 1333-1336.

Cody, G. D., Ade, H., Alexander, C. M. O., Araki, T., Butterworth, A., Fleckenstein, H., Flynn, G., Gilles, M. K., Jacobsen, C., Kilcoyne, A. L. D., Messenger, K., Sandford, S. A., Tyliszczak, T., Westphal, A. J., Wirick, S. & Yabuta, H. (2008) Quantitative organic and light-element analysis of comet 81P/Wild 2 particles using C-, N-, and O-mu-XANES. *Meteoritics & Planetary Science,* **43,** 353-365.

Cody, G. D., Ade, H., Wirick, S., Mitchell, G. D. & Davis, A. (1998) Determination of chemical-structural changes in vitrinite accompanying luminescence alteration using C-NEXAFS analysis. *Organic Geochemistry,* **28,** 441-455.

Cody, G. D., Brandes, J., Jacobsen, C. & Wirick, S. (2009) Soft X-ray induced chemical modification of polysaccharides in vascular plant cell walls. *Journal of Electron Spectroscopy and Related Phenomena,* **170,** 57-64.

Davidson, S. R. H. & Sherar, M. D. (2003) Measurement of the thermal conductivity of polyacrylamide tissue-equivalent material. *International Journal of Hyperthermia,* **19,** 551-562.

De Gregorio, B. T., Stroud, R. M., Nittler, L. R., Alexander, C. M. O., Kilcoyne, A. L. D. & Zega, T. J. (2009) Isotopic anomalies in organic nanoglobules from Comet 81P/Wild 2: Comparison to Murchison nanoglobules and isotopic anomalies induced in terrestrial organics by electron irradiation. *Geochimica Et Cosmochimica Acta,* **74,** 4454-4470.

Drouin, D., Couture, A. R., Joly, D., Tastet, X., Aimez, V. & Gauvin, R. (2007) CASINO V2.42 - A Fast and Easy-to-use Modeling Tool for Scanning Electron Microscopy and Microanalysis Users. *Scanning,* **29,** 92-101.

Edwards, H.K., Fay, M.W., Anderson, S.I., Scotchford, C.A., Grant, D.M. & Brown, P.D. (2009) An appraisal of ultramicrotomy, FIBSEM and cryogenic FIBSEM techniques for the sectioning of biological cells on titanium substrates for TEM investifation. *J. Microsc.* **234**, 16-25.

Fischione (2011) http://www.fischione.com.Fischione Instruments, Export, PA. Last accessed 1/3/2011.

Giannuzzi, L.A., Drown, J.L., Brown, S.R., Irwin, R.B. & Stevie, F.A. (1997) Focused-Ion-Beam Milling and Micromanipulation Lift-Out for Site-Specific-Cross-Secion TEM Specimen Preparation. *Mat. Res. Soc. Symp. Proc.* **480**, 19-27.

Giannuzzi, L.A., Geurts, J. & Ringnalda, J. (2005) 2 keV Ga$^+$ FIB Milling for Reducing Amorphous Damage in Silicon. *Microsc. Microanal.* **11**(S2), 828-829.

Giannuzzi, L. A. & Stevie, F. A. (2005) *Introduction to focused ion beams : instrumentation, theory, techniques, and practice,* Springer, New York.

Heaney, P. J., Vicenzi, E. P., Giannuzzi, L. A. & Livi, K. J. T. (2001) Focused ion beam milling: A method of site-specific sample extraction for microanalysis of Earth and planetary materials. *American Mineralogist,* **86,** 1094-1099.

Herrin, J. M. & Deming, D. (1996) Thermal conductivity of US coals. *J. Geophys. Res.-Solid Earth,* **101,** 25381-25386.

Hitchcock, A. P., Dynes, J. J., Johansson, G., Wang, J. & Botton, G. (2008) Comparison of NEXAFS microscopy and TEM-EELS for studies of soft matter (vol 39, pg 311, 2008). *Micron,* **39,** 741-748.

Jacobsen, Wirick, Flynn & Zimba (2000) Soft X-ray spectroscopy from image sequences with sub-100 nm spatial resolution. *Journal of Microscopy,* **197,** 173-184.

Jacobsen, C., Kirz, J. & Williams, S. (1992) Resolution in soft X-ray microscopes. *Ultramicroscopy,* **47,** 55-79.

Jacobsen, C., Williams, S., Anderson, E., Browne, M. T., Buckley, C. J., Kern, D., Kirz, J., Rivers, M. & Zhang, X. (1991) DIFFRACTION-LIMITED IMAGING IN A SCANNING-TRANSMISSION X-RAY MICROSCOPE. *Optics Communications,* **86,** 351-364.

Kaznatcheev, K. V., Karunakaran, C., Lanke, U. D., Urquhart, S. G., Obst, M. & Hitchcock, A. P. (2007) Soft X-ray spectromicroscopy beamline at the CLS: Commissioning results. In: *14th National Conference on Synchrotron Radiation Instrumentation.* Elsevier Science Bv, Baton Rouge, LA.

Kim, S. & Minor, A. (2008) FIB preparation of cross-sectional polymer thin film TEM samples. *Microscopy and Microanalysis,* **14,** 996-997.

Marko, M., Hsieh, C., Moberlychan, W., Mannella, C. A. & Frank, J. (2006) Focused ion beam milling of vitreous water: prospects for an alternative to cryo-ultramicrotomy of frozen-hydrated biological samples. *Journal of Microscopy-Oxford,* **222,** 42-47.

Marko, M., Hsieh, C., Schalek, R., Frank, J. & Mannella, C. (2007) Focused-ion-beam thinning of frozen-hydrated biological specimens for cryo-electron microscopy. *Nature Methods,* **4,** 215-217.

Mayer, J., Giannuzzi, L.A., Kamino, T. & Michael, J. (2007) TEM Sample Preparation and FIB-Induced Damage. *MRS Bull.* **32,** 400-407.

McCaffrey, J. P., Phaneuf, M. W. & Madsen, L. D. (2001) Surface damage formation during ion-beam thinning of samples for transmission electron microscopy. *Ultramicroscopy,* **87,** 97-104.

Meyer, B. (1976) Elemental sulfur. *Chemical Reviews,* **76,** 367-388.

Obst, M., Gasser, P., Mavrocordatos, D. & Dittrich, M. (2005) TEM-specimen preparation of cell/mineral interfaces by Focused Ion Beam milling. *American Mineralogist,* **90,** 1270-1277.

Orloff, J. (2009) Private Communication.

Overwijk, M.H.F., van der Heuvel, F.C. & Bulle-Lieuwma, W.T. (1993) Novel scheme for the preparation of transmission electron microscopy specimens with a focused ion beam. *J. Vac. Sci. Technol. B,* **11**, 2021-2024.

Schiffbauer, J. D. & Xiao, S. H. (2009) NOVEL APPLICATION OF FOCUSED ION BEAM ELECTRON MICROSCOPY (FIB-EM) IN PREPARATION AND ANALYSIS OF MICROFOSSIL ULTRASTRUCTURES: A NEW VIEW OF COMPLEXITY IN EARLY EUKARYOTIC ORGANISMS. *Palaios,* **24,** 616-626.

Stöhr, J. (1992) *NEXAFS spectroscopy,* Springer-Verlag, Berlin ; New York.

Warwick, T., Franck, K., Kortright, J. B., Meigs, G., Moronne, M., Myneni, S., Rotenberg, E., Seal, S., Steele, W. F., Ade, H., Garcia, A., Cerasari, S., Delinger, J., Hayakawa, S., Hitchcock, A. P., Tyliszczak, T., Kikuma, J., Rightor, E. G., Shin, H. J. & Tonner, B. P. (1998) A scanning transmission x-ray microscope for materials science spectromicroscopy at the advanced light source. *Review of Scientific Instruments,* **69,** 2964-2973.

Weber, P. K., Graham, G. A., Teslich, N. E., Chan, W. M., Ghosal, S., Leighton, T. J. & Wheeler, K. E. (2010) NanoSIMS imaging of Bacillus spores sectioned by focused ion beam. *Journal of Microscopy-Oxford,* **238,** 189-199.

White, H., Pu, Y., Rafailovich, M., Sokolov, J., King, A. H., Giannuzzi, L. A., Urbanik-Shannon, C., Kempshall, B. W., Eisenberg, A., Schwarz, S. A. & Strzhemeckny, Y. M. (2001) Focused ion beam/lift-out transmission electron microscopy cross sections of block copolymer films ordered on silicon substrates. *Polymer,* **42,** 1613-1619.

Wirick, S., Flynn, G. J., Keller, L. P., Nakamura-Messenger, K., Peltzer, C., Jacobsen, C., Sandford, S. & Zolensky, M. (2009) Organic matter from comet 81P/Wild 2, IDPs, and carbonaceous meteorites; similarities and differences. *Meteoritics & Planetary Science,* **44,** 1611-1626.
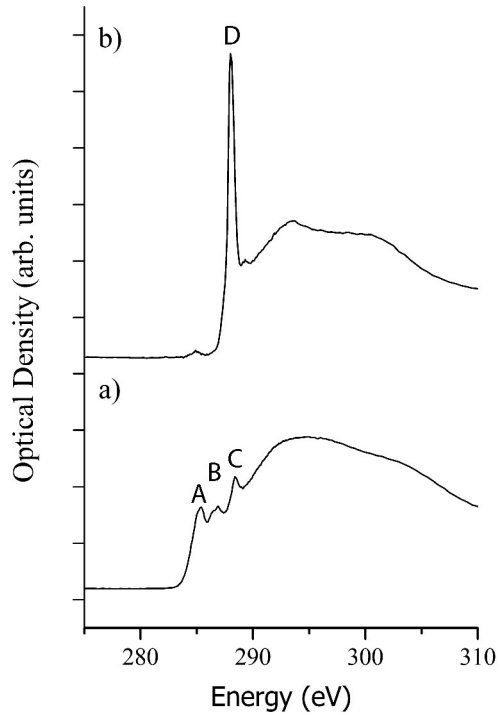
Figure 1

Figure 1: Carbon K XANES Spectra from microtomed samples: a) lignite coal and b) PAAm. Uppercase letters denote $1s \rightarrow \pi^*$ photoabsorption peaks corresponding to A) aromatic (or olefinic) C=C at 285.2 eV, B) Aromatic ketone $C_{aromatic}$-C=O at 286.6 eV, C) carboxyl carbonyl -(C=O)OH at 288.5 eV, D) Amide NH_2-C=O at 288.0 eV functional groups.
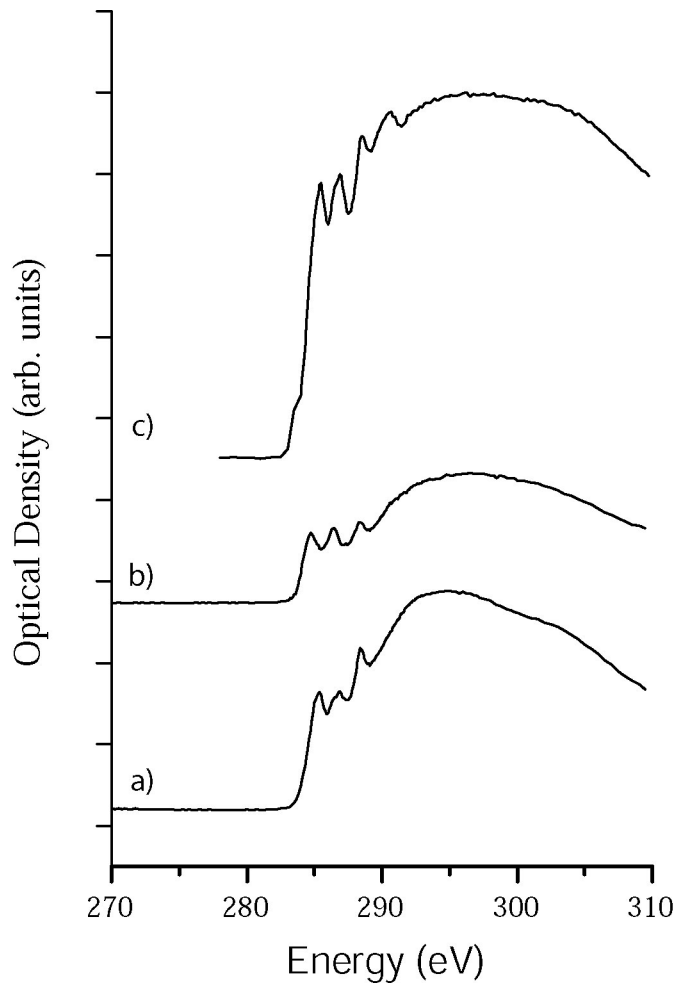
Figure 2

Fig 2: Comparison of a) microtomed coal, b) FIB-prepared coal with a 30 kV final ion polish with 5 keV electron beam irradiation, and c) FIB-prepared coal with a 30 kV final polish with no electron beam irradiation.

Figure 3
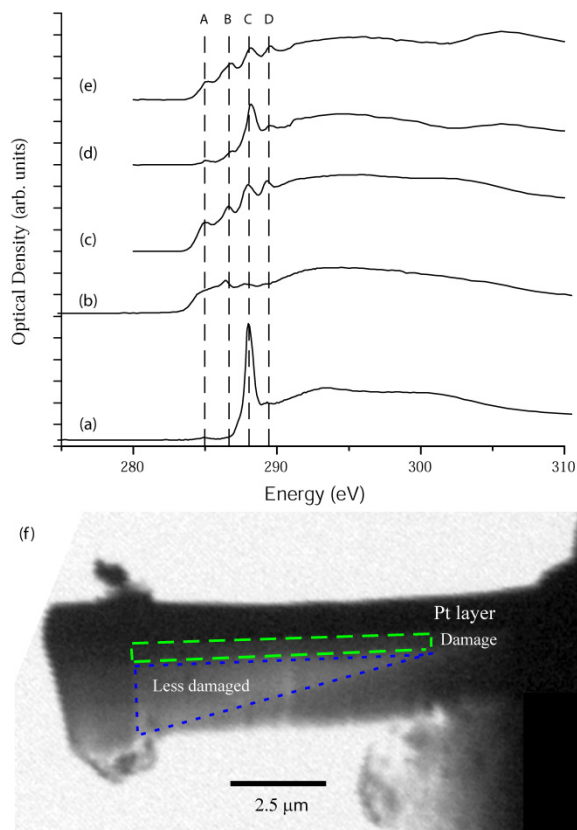
Figure 3: Electron beam damage effects on PAAm: XANES spectra of a) "pristine" microtomed PAAm, b) a FIB sample prepared using 30kV Ga$^+$ ions and imaged with 5 keV electrons during milling, c) a FIB sample prepared using 30 kV ions and imaged with 1 keV electrons during milling, d) a FIB sample prepared with no electron beam imaging, except for the top surface, generated from the sample region outlined in blue in (f), and e) the same sample as (d) but generated from the top portion of the sample that had been exposed to the 5 keV electron beam prior to Pt deposition and milling. Peak labels are A: aromatic C=C (285.0 eV), B: nitrile C≡N (286.6 eV), C: amide CONH$_x$ (288.0 eV), and D: imine C=N (289.2 eV) ; f) STXM image obtained at 280 eV showing two regions with distinct functional chemistry: an area that never experienced electron irradiation (blue outline; XANES spectrum shown in (d)) and a top surface layer that was irradiated during sample navigation (green outline; XANES spectrum shown in (e)). FIB/electron beam platinum has been deposited above the damaged surface layer and to the right of the sample is the post of a grid to which the sample was attached.
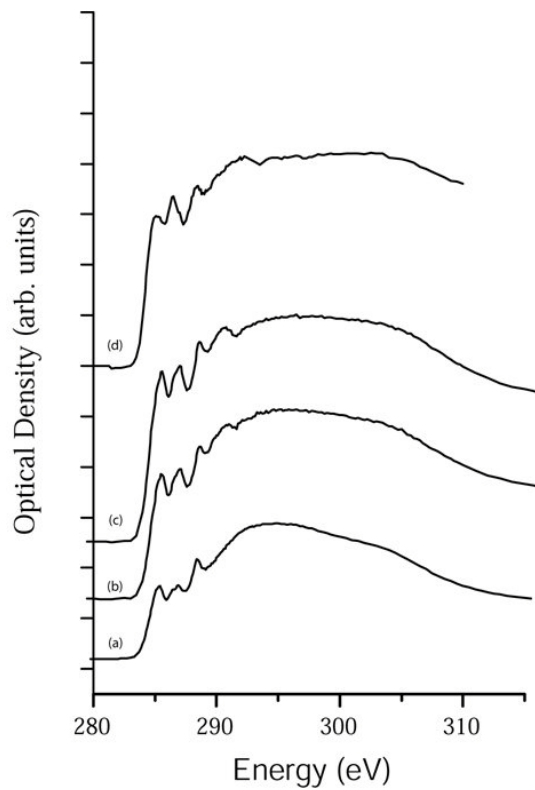
Figure 4

Figure 4: Carbon XANES spectra from coal samples showing the affects of varied voltage under cryogenic conditions: a) "pristine" microtomed sample, b) cryo-FIB section with 5 kV and 2 kV final polishing, c) cryo-FIB section with a 30 kV final polish, d) FIB sample with a 500 V final polish in a Fischione Nanomill at liquid nitrogen temperature. None of these samples were exposed to an electron beam.
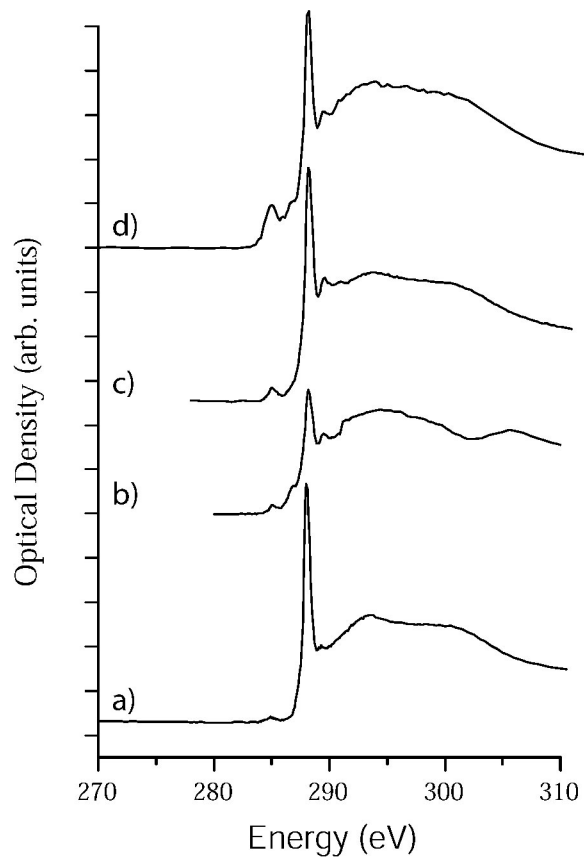
Figure 5

Figure 5: Carbon XANES spectra of PAAm showing the effect varying final polishing voltage: a) "pristine" microtomed sample, b) FIB-prepared sample with a 1 kV final polish, c) FIB-prepared sample with a two-step (5 kV and 2 kV) final polish, d) FIB-prepared sample with a "standard" 30 kV final polishing voltage. All samples have been prepared without visualizing with the electron beam.
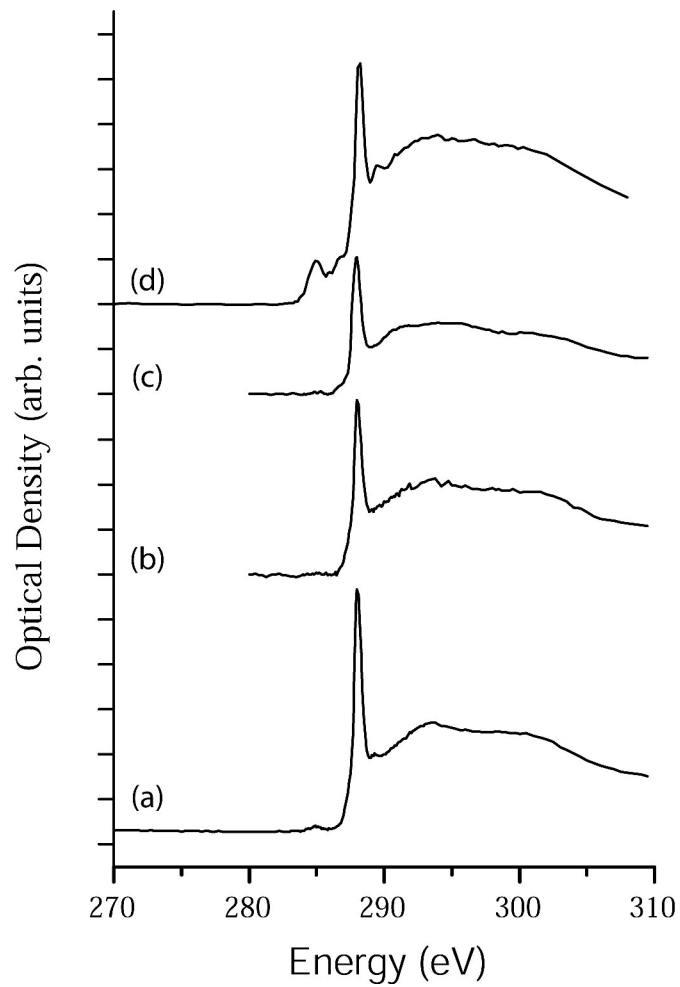
Figure 6

Figure 6: XANES data from microtomed PAAm that had been heated to various temperatures : a) unheated PAAm; b) sample that had been vacuum annealed at 128 ℃, c) sample that had been annealed at 231 ℃; d) FIB-prepared PAAm with no SEM imaging (previously shown in Figure 5d) and 30 keV final thinning voltage.
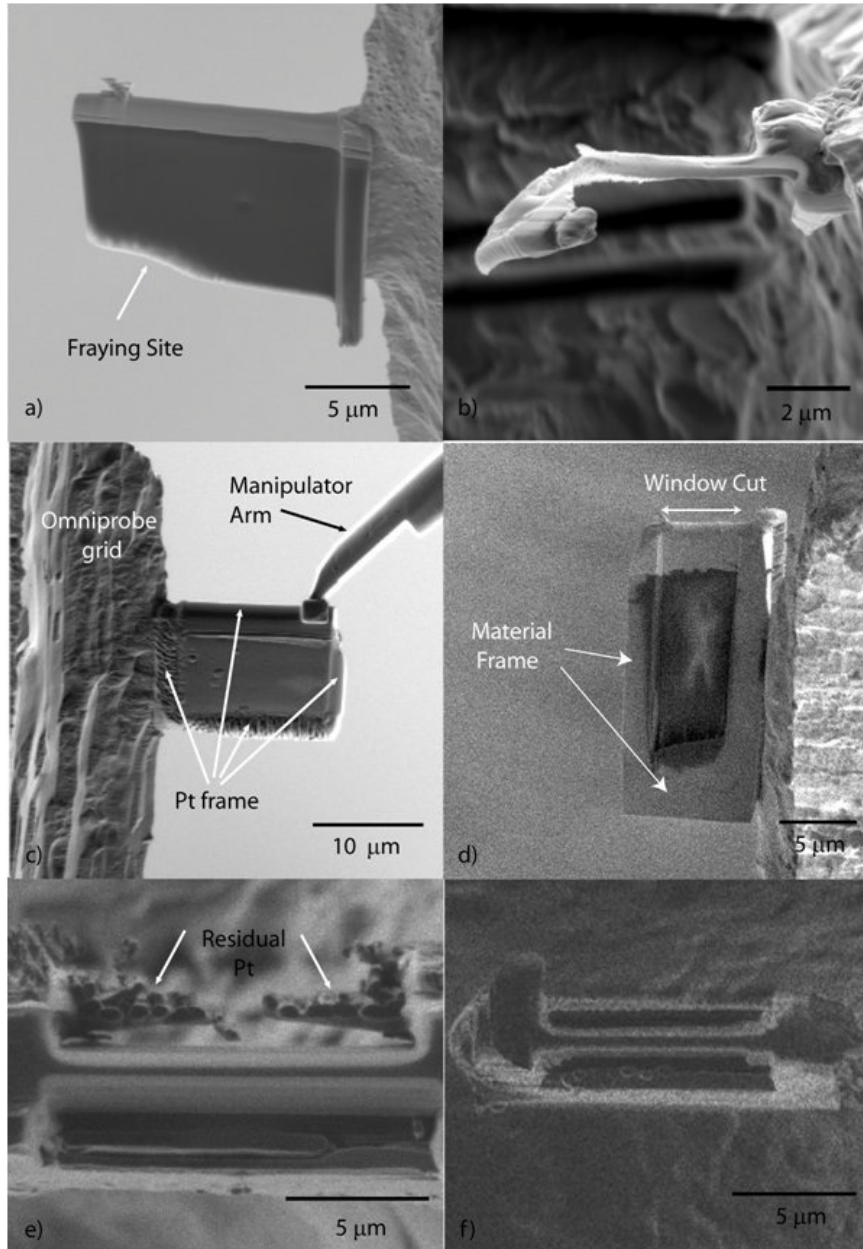
Figure 7

Figure 7: Effects and mitigation of sample softening in the FIB. a) Side view of a PAAm section that is beginning to degrade and warp b) Top view of the same section after additional FIB milling. Section rigidity may be maintained by either a c) Pt frame configuration or a d) natural frame surrounding the section. Top views of sections supported by e) a Pt Frame and f) a natural frame.
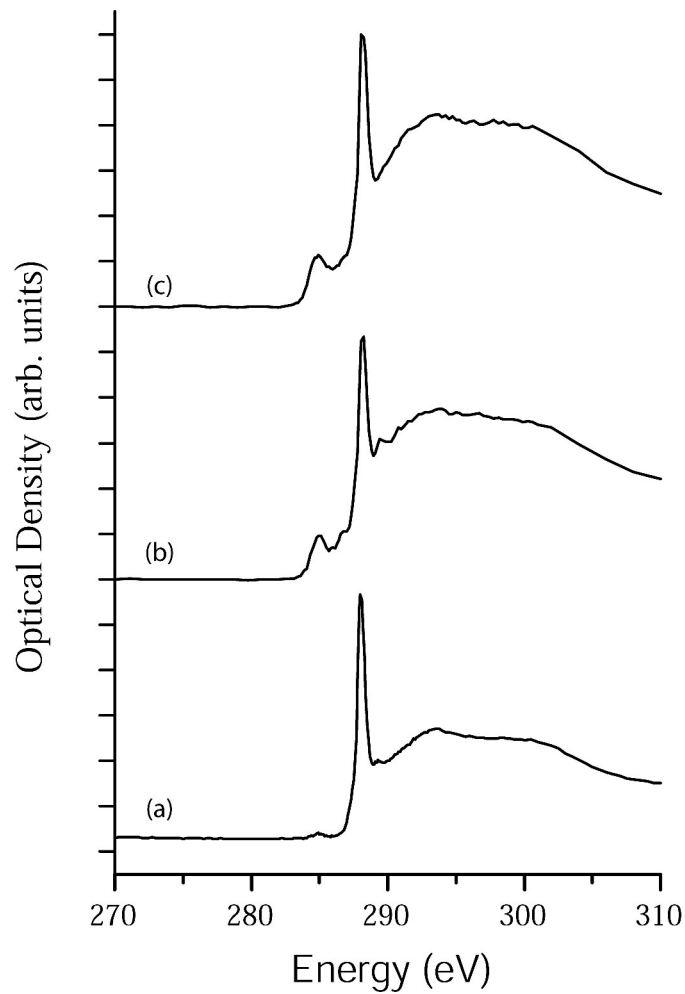
Figure 8

Figure 8: Carbon XANES spectra of PAAm prepared with various values of ion beam overlap: a) pristine microtome section, b) sample processed with 0% beam overlap, and c) sample processed with 50 % beam overlap (previously shown in Figure 5D). The final milling steps for the FIB sections were prepared without SEM imaging and a final ion current of 30 pA.